NUCLEAR THEORY, Vol. 39 (2022)
eds. M. Gaidarov, N. Minkov, Heron Press, Sofia

The Equation of State of Neutron-Rich Matter at Fourth Order of Chiral Effective Field Theory and the Radius of a Medium-Mass Neutron Star

F. Sammarruca

University of Idaho, 83844 Moscow Idaho, USA

Abstract. The equation of state of neutron-rich matter is at the forefront of nuclear astrophysics because of its role in shaping the properties of neutron stars. Recently, interest in compact stars has increased considerably as we have entered the "multi-messenger era" of astrophysical observations. The recent GW170817 neutron star merger event has yielded new and independent constraints on the radius of the canonical mass neutron star. Astronomy with gravitational waves provides additional opportunities to explore these exotic systems and other yet unknown regimes in the Cosmos. We discuss neutron star predictions based on our most recent equations of state. These are derived from chiral effective field theory, which allows for a systematic development of nuclear forces, order by order. We utilize high-quality two-nucleon interactions and include all three-nucleon forces up to fourth order in the chiral expansion.

1 Introduction

Neutron stars (NS) are intriguing systems. For one thing, NS studies reach out to all the fundamental forces in nature. Also, they offer the opportunity to study matter under conditions not typically encountered in terrestrial laboratories. The equation of state (EoS) of both neutron matter (NM) and symmetric nuclear matter (SNM), and the closely related symmetry energy, play a paramount role in stellar structure.

A neutron star is the remnant collapsed core of a giant star which has undergone a supernova explosion. Only stars with sufficient mass, estimated to be between 8 and 25 $M_\odot$, undergo a supernova event at the end of their life cycle. Due to its extremely compact nature, the neutron star is directly supported against further gravitational collapse into a black hole by mechanisms of nuclear origin, which make these objects excellent natural laboratories for exploring the nuclear equation of state (EoS).

The mass-radius relationship of neutron stars is uniquely determined from the star's EoS and thus reliable observational constraints can shed light on the EoS. While the radius cannot be directly measured, the mass of neutron stars in binary systems can be inferred from observation together with application of

gravitational theory. With constraints on the mass of a star, the Doppler shift is one way to estimates the radius. The neutron star radius is not measured directly, but observational data allow for indirect inference. Observation-based constraints consistently place the estimated radius of a neutron star in the range of 10-15 km. For instance, using accreting and bursting sources, the radius of the canonical-mass neutron star was determined to be within a range of 10.4 to 12.9 km [1], while analysis from the LIGO/Virgo observations determined the radius to be between 11.1 and 13.4 km [2]. Upper limits on the neutron star radii, as determined from iron emission lines, were placed between 14.5 and 16.5 km [3].

Neutron star models are generally in good agreement with observational constraints for the radius. For instance, the radius of the canonical-mass neutron star predicted from the set of EoS applied in Ref. [4] is predicted to be in the range 10.45–12.66 km. From a variety of techniques, based on experimentally determined quantities correlated to symmetry energy parameters, the radius is determined to be between 10.7 to 13.1 km [4–7], while using a range of theoretical models a limit of 9.7 to 13.9 km is obtained [4, 8, 9]. Recent surveys of neutron star physics and theoretical approaches include Refs. [10–12]. Exotic matter in stars is addressed, for instance, in Ref. [13].

The predictions discussed here are based on Refs. [14–16]. When discussing predictions and constraints, we emphasize the importance of ab initio *vs.* phenomenological approaches.

2 The Nuclear Physics Input

The EoS for neutron and symmetric matter are obtained at the leading-order in the hole-line expansion – namely, *via* a non-perturbative calculation of the particle-particle ladder. The single-particle potentials are computed self-consistently with the G-matrix, employing a continuous spectrum.

2.1 The two-nucleon force

The two-nucleon forces (2NF) we apply are from Ref. [17], a family of high-quality potentials from leading order (LO) to fifth order ($\mathrm{N^4LO}$) of the chiral EFT. The interactions in this set are more internally consistent than those from the previous generation [18]. Furthermore, the long-range part of these potentials is tightly constrained by the πN low-energy constants (LECs) from the Roy-Steiner analysis of Ref. [19]. This analysis is sufficiently accurate to render errors in the πN LECs essentially negligible for the purpose of quantifying the uncertainty.

2.2 The three-nucleon force

In the framework of the Δ-less chiral EFT (which we apply), The first occurence of three-nucleon forces (3NF) is seen at the third order. The leading 3NF consists of three components [20]: the long-range two-pion-exchange (2PE) graph,

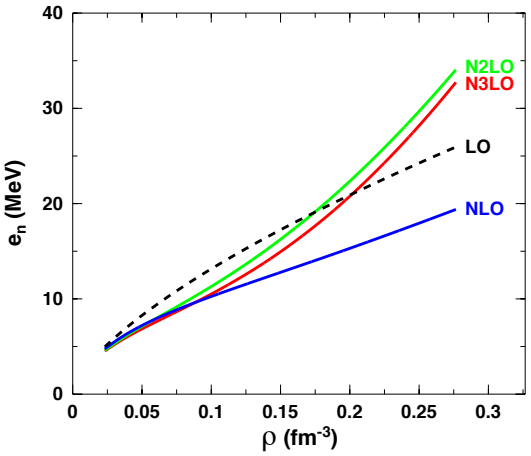

Figure 1. Energy per particle in neutron matter as a function of density from leading to fourth order of chiral perturbation theory. The cutoff is fixed at 450 MeV. The EoS are those obtained in Ref. [14].

which depends on LECs c_1, c_3, and c_4, the medium-range one-pion-exchange (1PE) diagram, carrying the LEC c_D, and a short-range contact term, containg the LEC c_E. We recall that the terms depending on c_4, c_D, and c_E do not contribute in neutron matter [21]. In infinite matter, it is possible to construct approximate expressions for the 3NF as density-dependent effective two-nucleon interactions as derived in Refs. [22, 23]. These can be written in terms of the well-known non-relativistic two-body nuclear force operators and, thus, can be easily implemented in the NN partial wave formalism for the G-matrix, which leads to the EoS.

We also include the subleading (N^{3}LO) 3NF, derived in Ref. [24, 25]. References [26–29] report applications of the subleading 3NF in some many-body systems. The long-range part of the 3NF at N^{3}LO includes: the 2PE topology, which is the longest-range contribution, the two-pion-one-pion exchange (2P1PE) topology, and the ring topology, which represents a pion being absorbed and reemitted from each of the three nucleons. We include relativistic corrections as well and find them to be very small (less than one MeV).

In Figure 1, we show the EoS in NM over four orders, from LO to N^{3}LO [14]. Large variations at low orders are of course not surprising, nor is the remarkable impact of the leading 3NF at N^{2}LO. The transition to fourth order brings in a slight increase in attraction, as was found from other EFT-based predictions [30].The overall convergence pattern is encouraging.

In Figure 2 an analogous presentation is provided for SNM. Similar considerations apply with regard to the order-by-order convergence pattern and the 3NF "signature" as in NM.

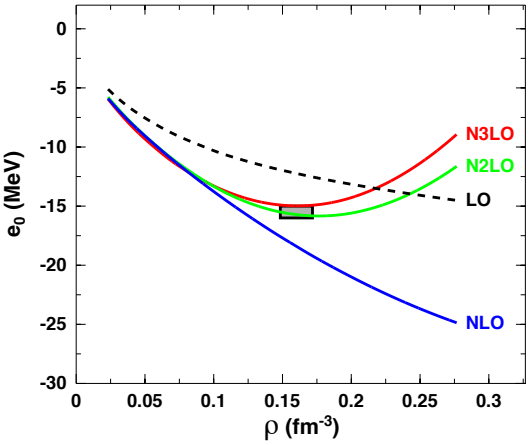

Figure 2. Energy per particle in symmetric nuclear matter as a function of density from leading to fourth order of chiral perturbation theory. The cutoff is fixed at 450 MeV. The shaded box marks the empirical saturation point. The EoS are the same as obtained in Ref. [15].

Once the EoS for NM and SNM are available, the EoS for stellar matter in β-equilibrium is easily obtained from the condition of energy minimization, subjected to the constraints of conserved nucleon density and global charge neutrality.

3 Polytropic Extrapolation

Chiral predictions have a limited domain of validity, which, in the previous section, we estimated to be about twice saturation density. The densities within neutron stars can reach five to six times saturation density, and therefore an appropriate method for extrapolating the EoS to these densities must be employed. To accomplish this, we express the high density pressure through polytropes [31]:

$$P(\rho) = \rho^2 \frac{\partial e_T(\rho)}{\partial \rho} = \alpha \rho^\Gamma \,, \tag{1}$$

where α is chosen such as to ensure continuity at the matching density. A comment is in place: while continuity of the pressure is of course preserved, additional considerations are necessary to ensure continuity of the derivative. The latter would be essential to implement thermodynamic consistency of the piecewise EoS, which is beyond our present scope. Note, further, that the presence of discontinuities in the polytropic index is not unusual for the purpose of describing the global features of the star [31]. Following Ref. [32], we match piecewise polytropes to the *ab initio* predictions as explained next.

The microscopic predictions reach a Fermi momentum of 1.6 fm^{-1}, which corresponds to 2.016 fm^{-1} in pure neutron matter at the same density,

$\rho = 0.277$ fm^{-3}. The standard practice is to ensure that the characteristic momentum of the system, p, divided by the cutoff, Λ, is a reasonable expansion parameter. Taking p to be the average momentum in a free Fermi gas of neutrons at the highest density we consider, we obtain a value of 68% for p/Λ, which is a pessimistic estimate, since the average momentum in β-stable matter is smaller than in pure NM. Having chosen the matching density, ρ_1, we join the pressure predictions with polytropes of different adiabatic index, ranging from 1.5 to 4.5. This range is chosen following guidelines from the literature, in particular Ref. [31], where constrains on phenomenologically parameterized neutron-star equations of state are investigated. To simulate a (likely) scenario where the pressure displays different slopes in different density regimes, we define a second matching density, ρ_2, approximately equal to $2\rho_1$, at which point a set of polytropes covering the same range of Γ is attached to each of the previous polytropes. This is illlustrated in Figure 3. It is important to emphasize that high-density EoS extrapolations are not meant to be a replacement for microscopic theoretical predictions [32] which, at this time, are not feasible at superhigh densities. Instead, the spreading of the high-density pressure values from the piecewise variation of the polytrope index allows to probe the sensitivity of lower-density predictions to the much larger uncertainty at high density.

To construct a physical EoS for high densities, we must apply additional constraints. One is the *causality limit*, which imposes the speed of sound in

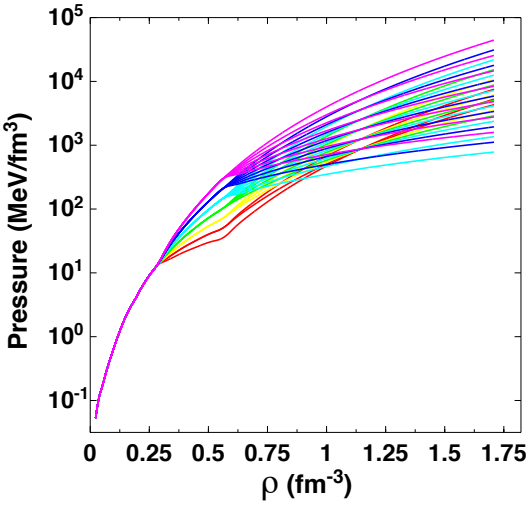

Figure 3. Pressure in β-stable matter as a function of density. The figure shows the spreading of the pressure values due to the matching of polytropes at two densities, $\rho_1 = 0.277$ fm^{-3} and $\rho_2 = 0.506$ fm^{-3}. Each group of curves with the same color contains EoSs with the same Γ_1 and varying Γ_2. The microscopic predictions (single pink curve prior to the first matching point), are obtained at N^{3}LO and cutoff equal to 450 MeV.

matter to be less than the speed of light. In terms of $P(\epsilon)$, the causality condition reads

$$\frac{dP(\rho)}{d\epsilon(\rho)} < 1\,. \tag{2}$$

Additionally we will only consider polytropes which can support a maximum mass of at least 2.01 $M_\odot$, to be consistent with the lower limit of the $(2.08 \pm 0.07)\ M_\odot$ observation reported in Ref. [33] for the J0740+6620 pulsar along with a radius estimate of (12.35 ± 0.75) km. To complete the EoS on the low-density side, we attach a crustal EoS [34, 35].

With the EoS available over a full range of densities, we obtain the mass-radius relation in a neutron star by solving the relativistic equations for hydrostatic equilibrium, the TOV equations [36, 37], from which the mass-radius relationship emerges for a given input EoS.

3.1 Results

To offer the reader a broader overview, we show in Table 1 the value of the symmetry energy and the slope parameter L with their uncertainty, where L is defined as

$$L = 3\rho_o \Big(\frac{\partial e_{\rm sym}(\rho)}{\partial \rho}\Big)_{\rho_o}\,. \tag{3}$$

These values were shown in Ref. [14] and compared to recent constraints.

We proceed with pressure predictions. Figure 3 displays the pressure in stellar matter as a function of the number density. The various curves span the range of acceptable combinations of polytropes, as explained in Section 3.

The mean value and standard deviation are $(\bar{R}_{1.4} = 11.96 \pm 0.58)$ km. The same procedure is applied at the lower orders, LO to N^{2}LO – that is, the EoS at each order is extended with polytropes and the mean value of the radius is calculated. With radius predictions available from leading to fourth order, we determine the truncation error. Combining the truncation and extrapolation uncertainties in quadrature, we state our estimate of the radius as

$$R_{1.4} = (11.96 \pm 0.80)\ \text{km}\,, \tag{4}$$

in excellent agreement with the LIGO/Virgo range of 11.1 to 13.4 km [2].

Our result is within the range generally found with EoS based on chiral EFT, which is 10 km to 14 km [38, 39], accounting for additional theoretical uncertainties, such as those originating from the choice of the many-body method and

Table 1. The symmetry energy and the slope parameter at N^{3}LO at saturation density ρ_o. L is defined as in Eq. (3).

ρ_0 (fm^{-3})	$e_{\rm sym}(\rho_o)$ (MeV)	$L(\rho_o)$ (MeV)
0.16	31.3 ± 0.8	52.6 ± 4.0

the implementation of the 3NF [40–44]. Some sensitivity of $R_{1.4}$ to the matching density was found [45, 46]. Moving the matching density from ρ_0 to $2\rho_0$ changed the range to (9.4–12.3) km [46] and to (10.3–12.9) km [45]. In the present analysis, the first matching point is determined by the highest density we reach out with the EFT calculations – a natural matching point. As for the second matching density, the details of the extension at the higher densities has only a minor impact on $R_{1.4}$.

4 Conclusion

A fully microscopic EoS up to central densities of the most massive stars – potentially involving non-nucleonic degrees of freedom and phase transitions – is not within reach. Nevertheless, neutron stars are powerful natural laboratories for constraining theories of the EoS. One must be mindful about the theory's limitations and the best ways to extract useful information from the observational constraints. Concerning the latter, there is no doubt that *The golden age of neutron-star physics has arrived.* [47].

Recently, we developed EoS for NM and SNM based on high-quality 2NF at N^{3}LO and including all subleading 3NF. These were used to construct the symmetry energy and the EoS in β-equilibrated matter, from which proton and lepton fractions are easily extracted. The stellar matter EoS was then extended to densities inaccessible to chiral EFT by matching it with piecewise polytropes of different adiabatic index. From those combinations, we dropped the EoS which did not satisfy the maximum mass constraint. The causality condition is also applied.

Constraints on the radius of a medium-mass neutron star, $R_{1.4}$, are becoming more stringent, with the current uncertainty reported at about 2 km. Furthermore, $R_{1.4}$ is known to be sensitive to the pressure in neutron-rich matter near normal densities, accessible to modern effective field theories of nuclear forces. For these reasons, we focused on predicting $R_{1.4}$ with proper uncertainy quantification. From reports in the literature, our predicted range would increase by about 1 km on either side when additional theoretical uncertainties are included.

Based on our analysis, we are confident that the estimate given in Eq. (4), approximately (12 ± 1) km, is characteristic of EFT predictions based on high-quality 2NF and properly calibrated (leading and subleading) 3NF. The range currently cited for chiral EFT-based predictions of $R_{1.4}$ is between 10 km and 14 km, accounting for additional theoretical uncertanties. In fact, it is interesting to notice that the extensive analysis from Ref. [45], where 300,000 possible EoS were generated, provides a range for $R_{1.4}$ between 10.0 and 12.7 km, with 12.0 km being the most probable value. We recall that the outcome of PREX II gives 13.33 km as the lower limit for the radius – which is problematic to reconcile with a multitude of microscopic predictions [48].

In conclusion, we reiterate that gravitational wave astronomy offers new exciting opportunities for nuclear astrophysics. Even though chiral EFT cannot

reach out to the extreme-density and yet unkown regimes at the core of these remarkable stars, continuosly improved *ab initio* calculations of the nuclear EoS are an essential foundation for interpreting current and future observations in terms of microscopic nuclear forces.

Acknowledgements

This work was supported by the U.S. Department of Energy, Office of Science, Office of Basic Energy Sciences, under Award Number DE-FG02-03ER41270.

References

[1] A.W. Steiner, J.M. Lattimer, E.F. Brown, *Astrophys. J.* **765** (2013) L5.
[2] E. Annala, T. Gorda, A. Kurkela, A. Vuorinen, *Phys. Rev. Lett.* **120** (2018) 172703.
[3] E.M. Cackett, S. Bhattacharyya, J.E. Grindley, M. van der Klis, T.E. Strohmayer, J.M. Miller, J. Homan, M.C. Miller, R. Wijnands, *Astrophys. J.* **674** (2008) 1.
[4] J.M. Lattimer, A.W. Steiner, *Astrophys. J.* **784** (2014) 123.
[5] W.G. Newton, M. Gearheart, J. Hooker, B.A. Li, In: *Neutron Star Crust* Eds: C.A. Bertulani, J. Piekarewicz (Nova Science Pub. Inc.: Hauppauge, NY, USA, 2011) Chapter 12.
[6] M.B. Tsang, J.R. Stone, F. Camera, P. Danielewicz, S. Gandolfi, K. Hebeler, C.J. Horowitz, J. Lee, W.G. Lynch, Z. Kohley, et al., *Phys. Rev. C* **86** (2012) 015803.
[7] J.M. Lattimer, Y. Lim, *Astrophys. J.* **771** (2013) 51.
[8] A.W. Steiner, S. Gandolfi, *Phys. Rev. Lett.* **108** (2012) 081102.
[9] K. Hebeler, J.M. Lattimer, C.J. Pethick, A. Schwenk, *Astrophys. J.* **773** (2013) 11.
[10] M. Oertel, M. Hempel, T. Klähn, S. Typel, *Rev. Mod. Phys.* **89** (2017) 015007.
[11] G.F. Burgio, A.F. Fantina, In: *The Physics and Astrophysics of Neutron Stars (Astrophysics and Space Science Library Book 457)* Eds: L. Rezzolla, P. Pizzochero, D. Jones, N. Rea, I. Vidaa (Springer, 2018), pp. 255-335.
[12] I. Vidana, A short walk through the physics of neutron stars;(2018) arXiv:1805.00837.
[13] D. Blaschke, J. Schaffner-Bielich, H.J. Schulze, *Eur. Phys. J. A* **52** (2016) 71.
[14] F. Sammarruca, R. Millerson, *Phys. Rev. C* **104** (2021) 034308.
[15] F. Sammarruca, R. Millerson, *Phys. Rev. C* **104** (2021) 064312.
[16] F. Sammarruca, R. Millerson, *Universe* **8** (2022) 133.
[17] D.R. Entem, R. Machleidt, Y. Nosyk, *Phys. Rev. C* **96** (2017) 024004.
[18] D.R. Entem, R. Machleidt, *Phys. Rev. C* **68** (2003) 041001(R).
[19] M. Hoferichter, J.R. de Elvira, B. Kubis, U.-G. Meissner, *Phys. Rev. Lett.* **115** (2016) 192301; *Phys. Rep.* **625** (2016) 1.
[20] E. Epelbaum, A. Nogga, W. Glöckle, H. Kamada, U.-G. Meißner, H. Witala, *Phys. Rev. C* **66** (2002) 064001.
[21] K. Hebeler, A. Schwenk, *Phys. Rev. C* **82** (2010) 014314.
[22] J.W. Holt, N. Kaiser, W. Weise, *Phys. Rev. C* **79** (2009) 054331.
[23] J.W. Holt, N. Kaiser, W. Weise, *Phys. Rev. C* **81** (2010) 024002.
[24] V. Bernard, E. Epelbaum, H. Krebs, U.-G. Meißner, *Phys. Rev. C* **77** (2008) 064004.

[25] V. Bernard, E. Epelbaum, H. Krebs, U.-G. Meißner, *Phys. Rev. C* **84** (2011) 054001.
[26] I. Tews, T. Krüger, K. Hebeler, A. Schwenk, *Phys. Rev. Lett.* **110** (2013) 032504.
[27] C. Drischler, A. Carbone, K. Hebeler, A. Schwenk, *Phys. Rev. C* **94** (2016) 054307.
[28] C. Drischler, K. Hebeler, A. Schwenk, *Phys. Rev. Lett.* **122** (2019) 042501.
[29] K. Hebeler, H. Krebs, E. Epelbaum, J. Golak, R. Skibinski, *Phys. Rev. C* **91** (2015) 044001.
[30] C. Drischler, A. Carbone, K. Hebeler, A. Schwenk, *Phys. Rev. C* **94** (2016) 054307.
[31] J.S. Read, B.D. Lackey, B.J. Owen, J.L. Friedman, Phys. Rev. D **79** (2009) 124032.
[32] F. Sammarruca, R. Millerson, *J. Phys. G: Nucl. Part. Phys.* **46** (2019) 024001.
[33] M.C. Miller, et al., The Radius of PSR J0740+6620 from NICER and XMM-Newton Data; arXiv:2105.06979. [astro-ph.HE]
[34] B.K. Harrison, J.A. Wheeler, *Gravitation Theory and Gravitational Collapse* (Chicago, IL: University of Chicago, 1965).
[35] J.W. Negele, D. Vautherin, *Nucl. Phys.* **A207** (1973) 298.
[36] R.C. Tolmann, *Phys. Rev. C* **55** (1939) 364.
[37] J.R. Oppenheimer, G.M. Volkoff, *Phys. Rev. C* **55** (1939) 374.
[38] C. Drischler, J.W. Holt, C. Wellenhofer, *Annu. Rev. Nucl. Part.* **71** (2021) 403.
[39] K. Hebeler, J. Lattimer, C. Pethick, A. Schwenk, *Phys. Rev. Lett.* **105** (2010) 161102.
[40] W.H. Dickhoff, C. Barbieri, *Prog. Part. Nucl. Phys.* **52** (2004) 377.
[41] A. Rios, *Front. Phys.* **8** (2020) 387.
[42] I. Tews, S. Gandolfi, A. Gezerlis, A. Schwenk, *Phys. Rev. C* **93** (2016) 024305.
[43] D. Lonardoni, I. Tews, S. Gandolfi, A. Gezerlis, J. Carlson, *Phys. Rev. Res.* **2** (2020) 022033.
[44] J. Lynn, et al., *Phys. Rev. Lett.* **116** (2016) 062501.
[45] Y. Lim, J. Holt, *Eur. Phys. J. A* **55** (2019) 209.
[46] I. Tews, J. Carlson, S. Gandolfi, S. Reddy, *Astrophys. J.* **860** (2018) 149.
[47] A. Mann. *Nature* **579** (2020) 20.
[48] B.T. Reed, F.J. Fattoyev, C.J. Horowitz, J. Piekarewicz, Implications of PREX-II on the equation of state of neutron-rich matter; arXiv:2101.03193.